Available online at www.sciencedirect.com

ScienceDirect

materialstoday: PROCEEDINGS

Materials Today: Proceedings 2S (2015) S535 – S539

International Conference on Martensitic Transformations, ICOMAT-2014

Detection of yield point behavior by acoustic emission in thin films

X. Wang[a], E. K. Hermann Salje[a,b], X. Ding[a,*], J. Sun[a]

[a] *State Key Laboratory for Mechanical Behavior of Materials, Xi'an Jiaotong University, Xi'an 710049, China*
[b] *Department of Earth Sciences, University of Cambridge, Cambridge CB2 3EQ, UK*

Abstract

Fabrication of domain-boundary based thin-film devices needs to control the yield point of a strained/cooled ferroelastics. We show that such control is possible by acoustic emission measurements using an integrated detector system. Through molecular dynamics simulations, we find that in thin films, the potential energy reduction during the yield event can reach to 4 meV/atom, and generate strain of 0.005 at the surface which lead to detectable acoustic emission signals.

Selection and Peer-review under responsibility of the chairs of the International Conference on Martensitic Transformations 2014.

Keywords: acoustic emission, yield point, ferroelastic devices, jerks, avalanches

1. Introduction

Hierarchical domains in single crystals and thin films are often related to strain effects during (multi-) ferroic phase transformations and occur spontaneously near the transition point or under external strain conditions [1]. The importance of strain effects in magnetic films was pointed out by Pertsev [2], and the effect of the domain walls on the conductivity of bismuth ferrite [3] and WO_3 [4] is well established. In addition, the effect of domain nucleation becomes even more pertinent when we consider device applications where the domain *boundaries* constitute the functional element of the device. Typical examples are ferroelectric domain walls in non-polar matrices like $CaTiO_3$ or $SrTiO_3$ [5,6], superconducting ferroelastic domain walls in WO_3 [4] and magnetic domain walls in Cr [7] and other materials including flexing effects [8-10]. To fabricate such domain boundary devices one needs to optimize

* Corresponding author. Tel.: +86-29-82668610; fax: +86-29-82663453.
E-mail address: dingxd@mail.xjtu.edu.cn

Selection and Peer-review under responsibility of the chairs of the International Conference on Martensitic Transformations 2014.
doi:10.1016/j.matpr.2015.07.341

the density of domain boundaries. The highest concentration of domain boundaries, or the finest domain pattern, occurs when the yield point is just overcome and the macroscopic stress has collapsed [11-14]. Any further strain destroys domain boundaries and makes the device material less efficient. This correlation implies that the optimum condition for high domain boundary concentrations is at the yield point of the strain-stress curve. This requires that the yield point is monitored very carefully.

Here, in Fig.1 we sketch such a production --- monitoring device for the yield point in thin films: the substrate may be heated (or cooled) and expand (or shrink). The two grey layers are two substrates which are needed to apply the external field on the thin film device. The AE detector (with two Pt conducting layers and one piezoelectric layer) is deposited adjacent to the thin film device, to collect the acoustic emission (AE) signals during the yield event. In addition, one polymer layer is deposited between the piezoelectric monitor and the lower substrate, in order to avoid the influence of substrate deformation on the AE signals.

The fundamental idea of the proposed detection method is that: when the imposed strain on the device material (blue) passes the yield strain the material will generate the desired microstructure. This leads simultaneously to a potential energy change of the sample which is abrupt and occurs only during the yield process. This energy change occurs in jerks according to the nucleation and growth of each element in the complex domain pattern [11-14] and lead to acoustic signals which travel to the sample surface [14]. This effect is commonly observed in bulk samples and in very thick devices [15,16], here we argue that similar effects are likely in thin films when domain patterns form. The displacement of lateral surface (due to the jerks) is then transmitted to the adjacent piezoelectric film (indicated in red in Fig.1) which can then be used as acoustic emission detector measuring crackling noise related to the domain nucleation. The key for the acoustic emission measurement is that any continuous displacement change would lead to a weak background signal in the detector while abrupt jerks lead to short, intense pulses which can be monitored with very high sensitivity.

The question is then whether piezoelectric signals are strong enough to be detected at the sample surface. The detection limit can be calibrated from currently available acoustic emission detectors where the detection limit at the interface is a strain of 10^{-3}. In this paper we show that the amplitudes of interface strain between the sample and AE detector are commonly surpassed in ferroelastic materials in the yield region.

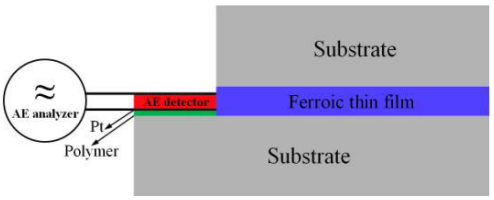

Fig. 1. Schematic device design for a ferroic thin film (blue) strained by two substrates (grey).The soft polymer layer (green) is used to reduce the effect of the substrate deformation on the AE signals collected by AE detector. When the yield point is crossed, the thin film will emit acoustic waves which couple to the piezoelectric detector (red).

2. Simulation method

We simulate the interfacial strain by a model for the ferroelastic transitions based on string mediated interactions [11-14]. The model used a generic two-body potential to represent the interactions of atoms in two-dimensional (2D) system. The potential energy $U(r)$ contains three parts, as the first-nearest atomic interactions of $10(r-1)^2$, the second-nearest interactions $-10(r-\sqrt{2})^2 + 2000(r-\sqrt{2})^4$ and the third-nearest interactions $-(r-2)^4$, where r is atomic distance. This potential is developed based on Landau theory by choosing the shear angle as "order parameter", and it is generic to all ferroelastic materials for studying twinning and mobility of twin boundaries. The details of properties obtained by this potential are described in our previous work [11-14]. The equilibrium unit cell is in shape of parallelogram with the shear angle of 4 degrees. The initial condition is a sandwich twinned structure containing two horizontal twin boundaries (shown in the insert figure of Fig.3(a)). The size of 2D simulation box is $200a \times 202a$ (20 nm × 20.2nm) in xy plane, where a (= 1 Å) is the lattice repetition unit. The system was first relaxed using a conjugate gradient refinement to find the optimal position for each lattice point. Molecular dynamics

was then performed to anneal the configuration at 0.1 K for 3×10^6 time steps. The only relaxations which occurred during the anneal were surface relaxations, no further microstructures developed. After this relaxation, the top and bottom three-layered atoms were fixed rigidly as the loading grip, and external strain was applied via a global shear of the two boundary layers. The shear was performed slowly over 3×10^6 time steps and output the data every 10 time steps. The temperature of the sample was held at $T = 0.1$ K by the Nosé-Hoover thermostat [17,18]. For comparison, the time scale of phonon excitation (one vibration) was about 50 time steps. All the calculations are performed using the LAMMPS code [19]. We use a constant strain rate (10^{-5} ps^{-1}) and then display our results as function of time to directly connect with the dynamics of acoustic emission.

3. Results

As the shear strain we applied will stabilize the top and bottom domain and destabilize the middle domain of the model, the unstable domain in the elastic region collapses into a multitude of twinned nanodomains during the yield region. Fig. 2 shows the evolution of microstructure during the yield region. Firstly a nuclei was generated at the pre-existed domain boundary (Fig. 2(a)) and then simultaneously grew to the free surface and the other pre-existed domain boundary (Figs. 2 (b)-(c)), and then the system form a complex domain pattern (Fig. 2d). We have chosen the temperature and boundary conditions so that the resulting yield pattern remains relatively simple and the lattice distortions are easy to follow in the computer simulation. Our yield pattern in Fig. 2(d) is simpler and contains fewer domain boundaries than those of larger samples [11-14] and can be seen as the worst case scenario for the proposed monitoring device.

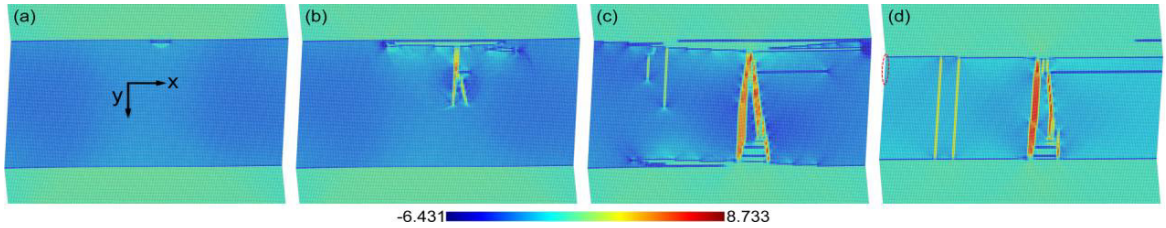

Fig. 2. Evolution of microstructure of a sandwich twinned model during the yield process. The color scheme relates to the shear angle between neighboring atoms, for details see references [11-14]. The middle domain (dark blue) contains some vertical and horizontal needle domains.

We now discuss details of the acoustic emission and the interfacial strain between the sample and the detector. As shown in Fig. 3(a), the increasing shear strain is initially compensated by an elastic deformation until a threshold is researched, after which the potential energy drops dramatically. The energy release of potential energy is integrated over the entire sample and is displayed in Fig. 3(b). The total reduction of potential energy is ~4 meV/atom and occurs over an initial time of ~4 ps (from t_1-t_3, the corresponding atomic configurations are shown in Fig.2(a)-2(c)). The relaxation tail in Fig.3(b) extends over some additional 25 ps (from t_3-t_4, the corresponding atomic configurations are shown in Figs. 2(c)-2(d)). The emitted kinetic energy of the event is shown in Fig. 3(b). The kinetic energy increases by 0.08 meV/atom at the yield point, indicating that the remaining potential energy is 3.92 meV/atom. This massive decrease of the potential energy leads to displacements which propagate to the surface and are observable as AE signals. The duration of the jerk is 4 ps with some additional relaxation which is much shorter than the rise time of the detector (e.g. some 100 ns). This means that the jerk profile does not relate to the nucleation event but displays simply the response function of the detection system. The kinetic energy is manifest in the enhanced phonon energy seen as 'ringing' of the sample as shown by the ripples in the kinetic energy (0.08 meV/atom) in Fig. 3(b). The related phonon pressure is relatively small and we thus expect that local thermal heating and thermal expansion do not lead to much displacement of the interface. We have tested the 'phonon cooling' on very fast shear rates and found non-isothermal effects only at much higher impact rates. Nevertheless, the kinetic energies in the simulations are useful for compare between different nano-structural changes and should not be used as absolute measures for the energy dissipation. The potential energy depends very little on the details of the simulation and we expect this value to be rather realistic for the assessment for the AE energies.

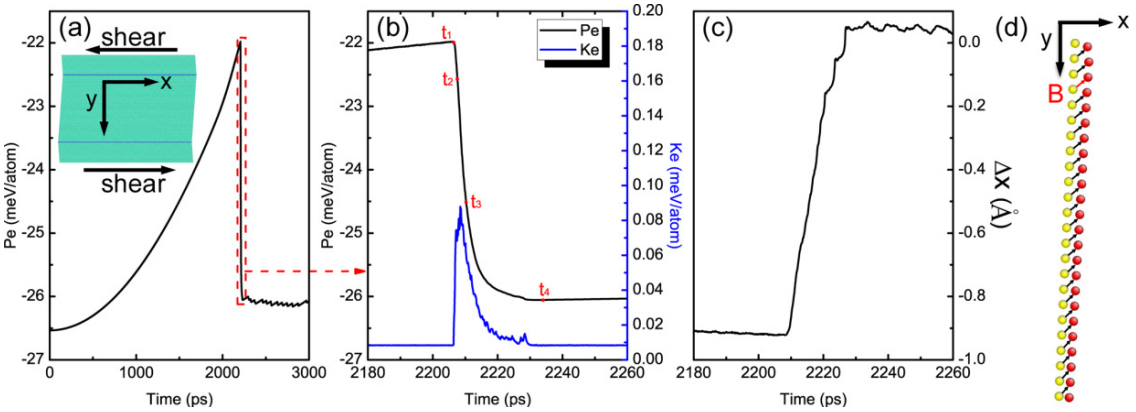

Fig. 3. (a) The change of potential energy Pe during the whole loading process; the inserted figure in (a) shows the initial model; a sudden collapse of potential energy Pe when the strain increases through the yield point, and the emission of kinetic energy Ke are shown in (b). The change in potential energy is large compared with the increase in kinetic energy, and the strain jerks to the detector are proportional to the change in potential energy. (c) shows the displacements of the surface atom B in x direction (hence at the interface with the piezoelectric detector, shown in (d)) ;and the position changes of surface atoms (highlighted by red ellipse in Fig.2(d)) are shown in (d).

We then compared the atomic positions of the sample before and after the yield event. Fig. 3(d) shows the surface atomic positions near the moving domain boundary in the upper part of the sample (highlighted by red ellipse in Fig. 2(d)). The longitudinal waves (inducing displacement along x axis) are largest near the moving domain boundaries in the upper and lower part of sample and extend to about one lattice unit. The displacements are not confined to the surface atoms (and hence the interface to the detector) but extend throughout the sample. The displacements of the surface atom B (in Fig. 3(d)) in x direction are shown in Fig. 3 (c). The maximum displacements at the surface are nearly one lattice repetition unit, i.e., the strain during the yield event is about 0.005 in our simulation. We can compare this value with measured AE signals at different transformation strains. Strong AE was found in the B2–R martensitic transformation of Ni–Ti–Fe with a spontaneous strain of 0.016 [20], while no AE signal was detected in the phase transition of $KMnF_3$ where the strain is $<< 10^{-3}$ [21]. These limits indicate that strain jerks of ~0.001 represent the lower limit for the sensitivity of current AE experiments. The proposed device is presumably more sensitive because the detector is directly linked with the sample with optimal acoustic coupling. The calculated yield strain of 0.005 should hence lead to a detectable acoustic signal. In addition, the electrical output in a test arrangement was simulated in [22], a resulting voltage of 10^{-3} V was found for similar displacements in our case and PZT as detector material. Furthermore, the signal is proportional to the total displacement, which is in turn proportional to the sample size, so that the final electrical signal will be sufficiently large to be observed. Details of design concepts are given in [23] with examples for application in [24].

We now compare our results with the sensitivity of previous acoustic emission measurements where the length of the sample is well defined. The best example is the collapse of porous materials [25] where the length of the sample is measured independently of the simultaneous acoustic emission. Taking the values given for the collapse of alumina in [25] we find that a contraction of a sample by 0.1 mm takes some 2000 seconds. The total activity of acoustic emission is some 10^4 counts per second. This leads to 2×10^8 counts/mm which extrapolates to some 20 counts per Angstrom contraction, which is the displacement in our simulation. The sample size is much bigger in the case of collapsing porous materials (some 40 mm^2 sample surface) but even a film with a reduced cross section by 100 would be AE active. Another experimental observation is the progression of an individual needle domain under external stress [26]. The fastest advancement that was observed optically was 20 m s^{-1}. This speed is similar to our simulated increase speed of the surface deformation of 0.05 Å ps^{-1}. Similar velocities were seen in ferroelectric materials [27] and the possible jerk emission was mentioned as ‘Barkhausen effect’ for such films in [28].

Finally, we noted that the sensitivity of our proposed device may be much better than the conventional acoustic emission devices for nanoindentation. In the conventional AE devices, the signal to noise ratio is low and the shape of the waveform and the rise time are susceptible to the coupling conditions between the AE sensor and the tested

material [29,30]. Although Tymiak and co-workers [31,32] obtained a higher AE signal by integrating a miniature AE sensor into the indenter tip, such device cannot continuously collect the AE signals unless the indenter tip can always be kept in contact with the sample surface.

4. Conclusion

In summary, we find that adding a (potentially sacrificial) piezoelectric thin film detector directly attached to a ferroelastic functional thin film is likely to be sensitive enough to detect the yield event of ferroelastic materials. The sensitivity may be largely enhanced in ceramic samples where the acoustic emission detector can simply be deposited as thin film on to the surface of the sample. Yield point activities are then seen as large bursts or jerks as well studied in the field of avalanche statistics.

Acknowledgements

We appreciate the support of NSFC (51171140, 51321003, 51320105014), and 111 project (B06025). EKHS is grateful for support by the Leverhulme fund (RPG-2012-564) and EPSRC (EP/K009702/1).

References

[1] J. Yao, W. Ge, L. Luo, J. Li, D. Viehland, H. Luo, Appl. Phys. Lett. 96 (2010) 222905.
[2] N.A. Pertsev, Appl. Phys. Lett. 102 (2013) 112407.
[3] P.E. Hopkins, C. Adamo, L. Ye, B.D. Huey, S.R. Lee, D.G. Schlom, J.F. Ihlefeld, Appl. Phys. Lett. 102 (2013) 121903.
[4] A. Aird, E.K.H. Salje, J. Phys.:Condens Matter. 10 (1998) L377–L380.
[5] S.V. Aert, S. Turner, R. Delville, D. Schryvers, G.V. Tendeloo, E.K.H. Salje, Adv. Mater. 24 (2012) 523 –527.
[6] E.K.H. Salje, O. Aktas, M.A. Carpenter, J.F. Scott, Phys. Rev. Lett. 111 (2013) 247603.
[7] R.K. Kummamuru, Y.-A . Soh, Nature 452 (2008) 859–863.
[8] E. Saitoh, H. Miyajima, T. Yamaoka, G. Tatara, Nature 432 (2004) 203 –206.
[9] J. Brooke, T.F. Rosenbaum, G. Aeppli, Nature 413 (2001) 610 –613.
[10] C. Gourdon, L. Thevenard, S. Haghgoo, A. Cebers. Phys. Rev. B 88 (2013) 014428.
[11] X. Ding, T. Lookman, Z. Zhao, A. Saxena, J. Sun, E.K.H. Salje, Phys. Rev. B 87 (2013) 094109.
[12] E.K.H. Salje, X. Ding, Z. Zhao, T. Lookman, A. Saxena, Phys. Rev. B 83 (2011) 104109.
[13] X. Ding, Z. Zhao, T. Lookman, A. Saxena, E.K.H. Salje, Adv. Mater. 24 (2012) 5385–5389.
[14] E.K.H. Salje, X. Wang, X. Ding, J. Sun, Phys. Rev. B 90 (2014) 064103.
[15] R. Niemann, J. Baró, O. Heczko, L. Schultz, S. Fähler, E. Vives, L. Mañosa, A. Planes, Phys. Rev. B 86 (2012) 214101.
[16] E. Vives, D.S. Parra, L. Mañosa, R. Romero, A. Planes, Phys. Rev. B 84 (2011) 060101.
[17] S. Nose, J. Chem. Phys. 81 (1984) 511 –519.
[18] W.G. Hoover, Phys. Rev. A 31 (1985) 1695–1697.
[19] S. Plimpton, J. Comput. Phys. 117 (1995) 1–19.
[20] E.K.H. Salje, H. Zhang, A. Planes, X. Moya, J. Phys.: Condens. Matter 20 (2008) 275216.
[21] W. Schranz, P. Sondergeld, V. Kityk, E.K.H. Salje, Phys. Rev. B 80 (2009) 094110.
[22] V.V. Amelichev, D.A. Saikin, V.M. Roshchin, M.V. Silibin, Semiconductors 44 (2010) 1631–1633.
[23] F. Mathieu, F. Larramendy, D. Dezest, C. Huang, G. Lavallée, S. Miller, C.M. Eichfeld, W. Mansfield, S. Trolier-Mckinstry, L. Nicu, Microelectron. Eng. 111 (2013) 68–76.
[24] P. Muralt, N. Ledermann, J. Baborowski, A. Barzegar, S. Gentil, B. Belgacem, S. Petitgrand, A. Bosseboeuf, N. Setter, IEEE Trans. Ultrason. Ferroelect. Freq. Contr. 52 (2005) 2276–2288.
[25] P.O. Castillo-Villa, J. Baro´, A. Planes, E.K.H. Salje, P. Sellappan, W.M. Kriven, E. Vives, J. Phys.: Condens. Matter. 25 (2013) 292202.
[26] R.J. Harrison, E.K.H. Salje, Appl. Phys. Lett. 97 (2010) 021907.
[27] V. Shur, E. Rumyantsev, S. Makarov, J. Appl. Phys. 84 (1998) 445–451.
[28] V.Y. Shur, J. Mater. Sci. 41 (2006) 199 –210.
[29] N.H. Faisal, R. Ahmed, R.L. Reuben, Int. Mater. Rev. 56 (2011) 98–142.
[30] D.F. Bahr, W. W. Gerberich, J. Mater. Res. 13 (1998) 1065–1074.
[31] N.I. Tymiak, A. Daugela, T.J. Wyrobek, O.L. Warren, J. Mater. Res. 18 (2003) 784–796.
[32] N.I. Tymiak, A. Daugela, T.J. Wyrobek, O.L. Warren, Acta Mater. 52 (2004) 553–563.